Metal-Dielectric transition in Sn-intercalated graphene on SiC(0001)

Y. R. Niu[1,2], A. A. Zakharov[2], R. Yakimova[3]

[1]School of Physics and Astronomy, Cardiff University, Cardiff, United Kingdom

[2]MAX IV Laboratory, Lund University, Lund, Sweden

[3]Department of Physics, Chemistry, and Biology (IFM), Linköping University, Linköping, Sweden

ABSTRACT

The Sn intercalation into a buffer layer graphene grown on 4H-SiC(0001) substrate has been studied with spectroscopic photoemission and low energy electron microscope. Both $SnSi_x$ and SnO_x interfacial layers are found to form below the buffer layer, converting it into a quasi-free-standing monolayer graphene. Combining the various operation modes of the microscope allows a detailed insight into the formation processes of the interlayers and their thermal stability. In particular, at the interface we observed a reversible transition from silicide to oxide after exposure to ambient pressure and subsequent annealing. This metal-dielectric transition might be useful for interface engineering in graphene-based devices.

1. Introduction

Epitaxial graphene grown on SiC substrates by thermal decomposition has attracted a lot of research interest in recent years [1–7]. As one of most promising methods of graphene fabrication, it is fully compatible with the modern semiconductor industrial standards, which means various graphene-based nanostructures and electronic/optoelectronic devices could be directly manufactured on a wafer-size graphene sample by lithography without being transferred onto other substrates [8–12]. The first carbon layer formed on a SiC(0001) surface (Si-face), so called buffer or zero layer, does not exhibit graphene-like electronic structure, i.e., Dirac points round the *K* points in the first Brillouin zone, because of the strong covalent bonds to the SiC substrate. Only the second carbon layer starts to show the properties of graphene and thus it is normally called a conventional monolayer graphene. The bonds between the buffer layer and SiC can be broken by intercalation of foreign atoms, which therefore converts the buffer layer to a monolayer graphene and opens a way to tailor its electronic properties, i.e., by doping. Intercalation of many species such as H, O, F, Au, Li, Na, Ge, Si and Yb [13–22] varied graphene doping in a wide range from n-doped to p-doped materials. Si and Ge, both from group IV, can be intercalated and effectively decouple the buffer layer from its supporting SiC substrate [19,20,23,24]. Si atoms can form two ordered structures at the interface

depending on the annealing temperature, and the more ordered one obtained at higher temperature passivates the substrate more effectively with less electron doping [23]. Ge, similar to Au [16], produces ambipolar doping depending on the amount of intercalated atoms [19,24]. The next element in the group, Sn, was found to decouple CVD graphene from its supporter, Ni(111), by forming a Sn/Ni ($\sqrt{3}\times\sqrt{3}$) alloy interface [25]. In the present work we study the intercalation of Sn into the buffer layer of SiC(0001) and investigate the property of the interfacial layer and quasi-free-standing graphene. We demonstrate this intercalation happens at temperatures above 600 ºC and the interfacial layer can be altered from metal to dielectric by exposing the sample to ambient conditions. We systematically characterized the intercalated graphene using a plethora of surface techniques offered by a synchrotron radiation-based spectroscopic photoemission and low energy electron microscope (SPELEEM): selected area low energy electron diffraction (μ-LEED), low energy electron microscopy (LEEM), x-ray photeoemission electron microscopy (XPEEM), selected area x-ray photoemission electron spectroscopy (μ-XPS) and selected area angle resolved photoemission electron spectroscopy (μ-ARPES).

2. Experimental procedures

The buffer layer graphene used in this study was grown on 4H-SiC(0001) substrates by a well-developed furnace method [7]. Briefly, the SiC wafer is annealed and graphitized through slow Si sublimation in an inductively heated furnace filled with an atmosphere Ar gas. Compared with annealing in ultra-high vacuum (UHV), the furnace method produces much larger graphene terraces and better crystallinity [26]. Before Sn deposition, the sample was degassed throughout in UHV at 600°C followed by a complete set of measurements to verify the attainment of a clean buffer layer. All measurements presented in this paper were carried out at the SPELEEM end station of Beamline I311, MAX IV Laboratory, Sweden [27]. Sn was deposited from a homemade evaporator that composes of a high purity Sn rod (99.99%) and a tungsten heating coil. The deposition rate was estimated to be about 0.14 monolayer/min from the attenuation of the substrate's Si2p spectra assuming a layer by layer growth of Sn. Here 1 monolayer (ML) is defined to be the C atom density of graphene, i.e., 0.382 atoms/$Å^2$. The values of mean free path used in the paper are adopted from Ref. [28]. During the deposition, half of the sample was covered by a Ta foil to keep it Sn-free. Thus comparative analyses can be done around the boundary between the Sn-free pristine buffer layer and the Sn-covered area to minimize any experimental uncertainties and artifacts. Most of the measurements were conducted at room temperature. The sample was heated by a tungsten filament build in the sample holder. For higher temperatures, e-beam bombardment was used by simply biasing the filament to a negative high voltage. The temperature was measured either by a W/Re3%-W/Re25% thermocouple spot-welded to the support ring under the sample or by an infrared pyrometer.

3. Results and discussion

After the deposition of about 0.7 ML Sn at room temperature, the sample was annealed step by step to 1050 °C. Our results (not shown) reveal that at about 600 °C, Sn atoms start to penetrate

and decouple the buffer layer from its SiC substrate. Figs. 1(a), 1(d) and 1(e) show LEEM and XPEEM images taken at the boundary separating Sn covered (right) and uncovered (left) halves of the sample after it was cooled down from 1050 °C. The difference between these two areas is well resolved from the corresponding μ-LEED patterns [Figs. 1(b) and 1(c)] and the XPEEM images taken at Si2p [Fig. 1(d)] and Sn4d photoelectrons [Fig. 1(e)]. The μ-LEED pattern from the intercalated area has much suppressed (if any) $6\sqrt{3}\times6\sqrt{3}R30°$ superstructure which signalizes that the buffer layer is lifted up and a quasi-free-standing graphene is formed. Further information is provided by the μ-XPS spectra of C1s, Si2p and Sn4d taken from the two areas [Figs. 1(f)–1(h)]. For the pristine buffer layer, its C1s spectrum consists of two surface components and one bulk SiC component [1]. After intercalation, the two surface components disappear while an intensive signal from the new formed graphene arises with a simultaneous reduction of the SiC component. In addition, the SiC component shifts to the lower binding energy by 1.6 eV, which is also well seen in earlier intercalation experiments with other intercalants carried out on the similar SiC-grown graphene samples [13,14,18–22]. Quite pronounced changes happen also in the Si2p spectra [Fig. 1(g)]. The original bulk Si2p component (SiC) was heavily reduced and shifted meanwhile for about the same amount (1.5 eV) in binding energy as the bulk C1s component shifts. A new component ($SnSi_x$) resulting from the interfacial Si atoms that now have bonds with intercalated Sn atoms emerges beside the bulk Si2p at lower binding energy. We denote this component as $SnSi_x$ for a precise stoichiometry is unknown. With quantitative comparison of these two Si2p components, we estimate that the thickness of interfacial Sn layer is about 3Å. This number can be understood on the basis of a model assuming a constant atomic volume maintains when metal atoms attach to a surface, for here, graphene [29]. For β-Tin with a body centered tetragonal structure, 4 atoms in a volume of $5.813\times5.813\times3.18$ Å^3, a Sn atom occupies 27.0488 Å^3 [30], which turns out that a single layer of such Sn atoms on graphene should be 10.323Å thick, provided the graphene lattice is 2.46 Å. Accordingly we can conclude that about 1/3 ML Sn was intercalated under the graphene, which is quite reasonable for about every third carbon atom in the buffer layer graphene forms a C-Si bond [1]. Here 1 ML corresponds to two Sn atoms per graphene unit cell. Finally, deconvolution of the Sn4d spectrum from the $SnSi_x$ intercalated area indicates a small number of Sn clusters exists on the top of the graphene. Such Sn clusters are also traceable on the buffer layer area as can be seen in Fig. 1(h).

Oxidation of the intercalated graphene was made by exposing it to the ambient pressure for about four months. After introduced into the UHV chamber, the sample was heated at 600 °C to remove any possible contamination. LEEM, Si2p and Sn4d XPEEM images of the boundary area after oxidation are shown in Figs. 2(a), 2(d) and 2(e). Atmospheric pressure of oxygen (or moisture) might be a prerequisite for this oxidation process because no oxidation can be found for the interfacial Sn layer by annealing the sample in situ at as high as 600 °C in an oxygen pressure of 5×10^{-6} torr (the highest gas pressure available in our UHV chamber). The μ-LEED pattern from the Sn-intercalated part after oxidation shows more diffuse (00) spots and even weaker $6\sqrt{3}\times6\sqrt{3}R30°$ and bulk SiC spots than that before oxidation [Figs. 2(b) and 2(c)]. Note that data presented in Fig. 2 are from a different preparation of the surface with a boundary area consisting of a mix of buffer layer and $SnSi_x$ intercalated graphene patches. To avoid

confusion, the μ-LEED patterns here and the corresponding μ-XPS data to be presented were collected ~150 μm away from the boundary. The boundary area will be discussed later.

After air exposure, the SiC component of C1s peak [Fig. 2(f)] moves back by 0.4 eV to higher binding energy which indicates the extra charge transfer between the substrate and the first carbon layer. After oxidation, no $SnSi_x$ component can be seen any more, which means the Sn bonds to Si are broken and replaced by oxygen. Moreover, the bulk Si2p component moves back to the higher binding energy by ~0.5 eV [Fig. 2(g)], which is consistent with the C1s shift of the substrate. Using a simple attenuation model to compare the Si2p spectrum of the pristine buffer layer with that after oxidation, we estimated that the interfacial SnO_x layer is about 11 Å thick. Note that the method used here is a rough estimation and its accuracy depends on many factors, i.e., the selection of mean free path of electrons, the film stoichiometry of Sn and O, and the atom arrangement in the interfacial layer. In addition to the changes of C1s and Si2p spectra, the Sn4d peak [Fig. 2(h)] shifts to the higher binding energy by 2.3 eV and exhibits considerable broadening after long time air exposure. The oxidation of Sn is also seen from the O1s spectrum in the inset of Fig. 2(h). Similar to the previous case of $SnSi_x$, we denote the Sn oxide hereafter as SnO_x due to the uncertain stoichiometry at the interface.

Having three different species (buffer layer, $SnSi_x$ and SnO_x) on the surface, it is important to easily distinguish them not only with X-rays but also with a diffraction contrast. To do that, we collected LEEM-IV curves of the pristine buffer layer, the buffer layer after oxidation, $SnSi_x$ and SnO_x intercalated graphene shown in Fig. 3, which give additional insight into the intercalation and oxidation process. The number of dips in the oscillated LEEM-IV curves has been used extensively as an easy and reliable way to count the number of graphene layers just by counting the number of dips in the reflectivity curve [31,32]. A typical LEEM-IV curve of the buffer layer doesn't show any pronounced dip due to its strong bonding to the substrate. Only the next layer of carbon, on top of the buffer layer, would cause a characteristic dip at about 3 eV. In our case, after the Sn intercalation, a pronounced dip appears at about 5 eV, which indicates a quasi-free-standing graphene as a result of intercalation. The LEEM-IV curve after Sn intercalation is indeed similar to that from an n-type Ge intercalated monolayer graphene formed by intercalation of about 1 ML Ge atoms into the interface [19]. It is also analogous to what was obtained from an n-type Au intercalated monolayer graphene with 1/3 ML Au present at the interface [16,33]. After Sn oxidation, an extra dip appears in the LEEM-IV curve at about 3 eV (Fig. 3). A similar dip was also found in the Ge and Au cases when more atoms were intercalated into the interface, i.e., 2 ML Ge and 1 ML Au respectively [19,33]. Thus this second dip is an indication of a further graphene layer lift up, which is not surprised for extra oxygen atoms go into the interface. Significant difference of Sn intercalation with regard to Ge and Au is the absence of the minimum at 7 eV and the preservation of the dip at 5 eV. Apparently, two different kinds of intercalated atoms coexisting at the interface are responsible for such a difference.

Now we turn to the electronic structures of the Sn-intercalated graphene. Valence band (VB) spectra from the pristine buffer layer, the $SnSi_x$ and SnO_x intercalated graphene are shown in Fig. 4(a). The main result of the present study is a significant density of electronic states at the

Fermi level (E_F) for $SnSi_x$ intercalated graphene. Such high electronic density of states is a characteristic of the metallic Sn-Si interface and has never been observed for other intercalants. Kim et al. [34] previously claimed the metallicity of this Sn-Si interface but the inferior quality of the buffer layer sample used with significant density of states at E_F before intercalation depreciates their statement. Peaks at binding energies of about 0.3, 1.2 and 2.6 eV may originate from the quantum well states due to the potential relief of the valence bands at the interface [35]. After oxidation, the states around E_F disappear which manifests a metal-dielectric transition in the system. The electronic states in the valence band at 3 and 5 eV get increased which is due to the contribution from Sn5s and O2p states [36].

The Dirac cone formed by the linear dispersive states around the *K* point in the first Brillouin zone is a well-known fingerprint of free-standing graphene. A three dimensional dataset of the band structures can be obtained by doing μ-ARPES measurement in the photoelectron diffraction mode of the microscope. After Sn intercalation, six clear Dirac cones close to E_F emerge as shown in Fig. 4(b). The band structures around the *K* point before and after oxidation are shown in Fig. 4(c). We found that the Dirac point after Sn intercalation locates roughly at E_F, which clearly demonstrates the graphene layer is neutral in terms of doping. The intrinsic n-doping due to the charge transfer from the SiC substrate that was normally observed in the conventional monolayer graphene, is not seen here. After oxidation the Dirac point moves downward by 0.4 eV which turns the graphene from neutral to n-doping. One possible explanation for such an electron transfer is the existence of oxygen vacancies in the interfacial SnO_x layer. It is worth to note that the spectra in Figs. 4(a) and 4(c) are collected in different parts of the Brillouin zone: VB spectra in Fig. 4(a) are acquired close to the zone center while spectra in Fig. 4(c) show the electronic structure around the *K* point.

One more interesting and important observation is the thermal stability of the Sn oxide under graphene. A closer inspection of the buffer layer area near the boundary in Figs. 2(a), 2(d) and 2(e) reveals that the area consists of a mixture of the buffer layer, SnO_x and $SnSi_x$ intercalated graphene, which can be seen also by the μ-XPS Sn4d spectrum from the boundary area [Fig. 2(h)]. Upon annealing the amount of the $SnSi_x$ intercalated graphene at the boundary gradually grows at the expense of small patches of the SnO_x which decompose at temperatures above 1000 ºC. The whole process can be followed in the stack of LEEM images [Figs. 5(a)–5(e)] taken after successive flashes at 1100 °C. A stripe-like area ($SnSi_x$) at the boundary constantly grows after every new flash and we couple this behavior with the decomposition of small SnO_x patches embedded in the buffer layer area and the consequent re-formation of metallic $SnSi_x$ intercalated graphene. In each LEEM image (Fig. 5), the three areas, from left to right, are buffer layer, restored $SnSi_x$ intercalated graphene and SnO_x intercalated graphene. The restored metallic graphene is almost identical to the graphene before oxidation, which has been verified by μ-LEED, μ-XPS, μ-ARPES and LEEM-IV curves. For example, in Fig. 5(f) the Si2p spectrum from the metallic ($SnSi_x$) area resembles the counterpart from Fig. 1(g). The Sn4d spectra shown in Fig. 5(g) are almost identical to the spectra before oxidation [Fig. 1(h)]. It is worth to mention that the SnO_x intercalated half of the sample [Figs. 5(a)–(e)] seems to stay intact during the repeated annealing, though an indication of SnO_x decomposition even from this area can be seen from Fig. 5(g) where the μ-XPS Sn4d data for two successive flashes

[Figs. 5(c) and (d)] show some decrease in SnO_x photoelectron intensity. This means that more energy (higher temperatures or longer flashes) is needed to decompose a continuous SnO_x layer back to the metallic state.

4. Conclusions

The process of Sn intercalation and reversible oxidation on a buffer layer graphene/SiC(0001) has been studied by various complementary microscopic techniques offered by the synchrotron radiation-based SPELEEM microscope. A Sn interfacial layer of about 1/3 ML thick forms at about 600 °C after Sn intercalation. This layer is metallic as can be inferred from the μ-XPS data showing significant density of the electronic states at E_F. This interfacial layer can be oxidized by long time ambient pressure exposure which turns the system to the dielectric state. We found that small insulating patches of the SnO_x intercalated graphene can be decomposed back to the metallic state by high temperature (1100 ºC) annealing. Our results pave the way to interface engineering of the Sn-intercalated graphene grown on SiC, utilizing the possible chemical reactions at the interface in this system. This idea is promising in the development of graphene-base devices, considering the extensive usage nowadays of Sn oxide in conductive glass and gas sensors.

Acknowledgement

The authors would like to thank Ernst Bauer and Kaibo Zheng for stimulating discussions as well as Jacek Osiecki for valuable technical suggestion.

References

[1] K. V. Emtsev, F. Speck, T. Seyller, L. Ley, J.D. Riley, Interaction, growth, and ordering of epitaxial graphene on SiC{0001} surfaces: A comparative photoelectron spectroscopy study, Phys. Rev. B - Condens. Matter Mater. Phys. 77 (2008) 1–10. doi:10.1103/PhysRevB.77.155303.

[2] K. V Emtsev, A. Bostwick, K. Horn, J. Jobst, G.L. Kellogg, L. Ley, J.L. Mcchesney, T. Ohta, S.A. Reshanov, J. Röhrl, E. Rotenberg, A.K. Schmid, D. Waldmann, H.B. Weber, T. Seyller, Towards wafer-size graphene layers by atmospheric pressure graphitization of silicon carbide, Nat. Mater. 8 (2009) 203–207. doi:10.1038/nmat2382.

[3] V. Jokubavicius, G.R. Yazdi, I.G. Ivanov, Y. Niu, A. Zakharov, T. Iakimov, M. Syväjärvi, R. Yakimova, Surface engineering of SiC via sublimation etching, Appl. Surf. Sci. 390 (2016) 816–822. doi:10.1016/j.apsusc.2016.08.149.

[4] H.C. Wu, A.N. Chaika, T.W. Huang, A. Syrlybekov, M. Abid, V.Y. Aristov, O. V. Molodtsova, S. V. Babenkov, D. Marchenko, J. Sánchez-Barriga, P.S. Mandal, A.Y. Varykhalov, Y. Niu, B.E. Murphy, S.A. Krasnikov, O. Lübben, J.J. Wang, H. Liu, L. Yang, H. Zhang, M. Abid, Y.T. Janabi, S.N. Molotkov, C.R. Chang, I. Shvets, Transport Gap Opening and High On-Off Current Ratio in Trilayer Graphene with Self-Aligned Nanodomain Boundaries, ACS Nano. 9 (2015) 8967–8975. doi:10.1021/acsnano.5b02877.

[5] R.M. Tromp, J.B. Hannon, Thermodynamics and kinetics of graphene growth on SiC(0001), Phys. Rev. Lett. 102 (2009) 1–4. doi:10.1103/PhysRevLett.102.106104.

[6] W. Norimatsu, M. Kusunoki, Epitaxial graphene on SiC{0001}: advances and perspectives., Phys. Chem. Chem. Phys. 16 (2014) 3501–11. doi:10.1039/c3cp54523g.

[7] G.R. Yazdi, T. Iakimov, R. Yakimova, Epitaxial Graphene on SiC : A Review of Growth, (2016). doi:10.3390/cryst6050053.

[8] A. Tzalenchuk, S. Lara-Avila, A. Kalaboukhov, S. Paolillo, M. Syväjärvi, R. Yakimova, O. Kazakova, T.J.B.M. Janssen, V. Fal'ko, S. Kubatkin, Towards a quantum resistance standard based on epitaxial graphene., Nat. Nanotechnol. 5 (2010) 186–9. doi:10.1038/nnano.2009.474.

[9] Y.-M. Lin, A. Valdes-Garcia, S.-J. Han, D.B. Farmer, I. Meric, Y. Sun, Y. Wu, C. Dimitrakopoulos, A. Grill, P. Avouris, K.A. Jenkins, Wafer-Scale Graphene Integrated Circuit, Science 332 (2011) 1294–1297. doi:10.1126/science.1204428.

[10] F. Wang, G. Liu, S. Rothwell, M.S. Nevius, C. Mathieu, N. Barrett, A. Sala, T.O. Menteş, A. Locatelli, P.I. Cohen, L.C. Feldman, E.H. Conrad, Pattern induced ordering of semiconducting graphene ribbons grown from nitrogen-seeded SiC, Carbon 82 (2015) 360–367. doi:10.1016/j.carbon.2014.10.081.

[11] J. Baringhaus, M. Ruan, F. Edler, A. Tejeda, M. Sicot, A. Taleb-Ibrahimi, A.P. Li, Z.G. Jiang, E.H. Conrad, C. Berger, C. Tegenkamp, W.A. de Heer, Exceptional ballistic transport in epitaxial graphene nanoribbons, Nature 506 (2014) 349–354. doi:Doi 10.1038/Nature12952.

[12] W.S. Hwang, P. Zhao, K. Tahy, L.O. Nyakiti, V.D. Wheeler, R.L. Myers-Ward, C.R. Eddy, D.K. Gaskill, J. a. Robinson, W. Haensch, H. (Grace) Xing, A. Seabaugh, D. Jena, Graphene nanoribbon field-effect transistors on wafer-scale epitaxial graphene on SiC substrates, APL Mater. 3 (2015) 11101. doi:10.1063/1.4905155.

[13] C. Riedl, C. Coletti, T. Iwasaki, A.A. Zakharov, U. Starke, Quasi-free-standing epitaxial graphene on SiC obtained by hydrogen intercalation, Phys. Rev. Lett. 103 (2009) 1–4. doi:10.1103/PhysRevLett.103.246804.

[14] S. Oida, F.R. McFeely, J.B. Hannon, R.M. Tromp, M. Copel, Z. Chen, Y. Sun, D.B. Farmer, J. Yurkas, Decoupling graphene from SiC(0001) via oxidation, Phys. Rev. B - Condens. Matter Mater. Phys. 82 (2010) 1–4. doi:10.1103/PhysRevB.82.041411.

[15] S.L. Wong, H. Huang, Y. Wang, L. Cao, D. Qi, I. Santoso, W. Chen, A.T.S. Wee, Quasi-free-standing epitaxial graphene on SiC (0001) by fluorine intercalation from a molecular source, ACS Nano. 5 (2011) 7662–7668. doi:10.1021/nn202910t.

[16] I. Gierz, T. Suzuki, R.T. Weitz, D.S. Lee, B. Krauss, C. Riedl, U. Starke, H. Höchst, J.H. Smet, C.R. Ast, K. Kern, Electronic decoupling of an epitaxial graphene monolayer by gold intercalation, Phys. Rev. B - Condens. Matter Mater. Phys. 81 (2010) 1–6. doi:10.1103/PhysRevB.81.235408.

[17] S. Watcharinyanon, L.I. Johansson, A.A. Zakharov, C. Virojanadara, Studies of Li intercalation of hydrogenated graphene on SiC(0001), Surf. Sci. 606 (2012) 401–406. doi:10.1016/j.susc.2011.10.023.

[18] C. Xia, S. Watcharinyanon, A.A. Zakharov, L.I. Johansson, R. Yakimova, C. Virojanadara, Detailed studies of Na intercalation on furnace-grown graphene on 6H-SiC(0001), Surf. Sci. 613 (2013) 88–94. doi:10.1016/j.susc.2013.03.011.

[19] K. V. Emtsev, A.A. Zakharov, C. Coletti, S. Forti, U. Starke, Ambipolar doping in

quasifree epitaxial graphene on SiC(0001) controlled by Ge intercalation, Phys. Rev. B - Condens. Matter Mater. Phys. 84 (2011) 1–6. doi:10.1103/PhysRevB.84.125423.

[20] C. Xia, S. Watcharinyanon, A.A. Zakharov, R. Yakimova, L. Hultman, L.I. Johansson, C. Virojanadara, Si intercalation/deintercalation of graphene on 6H-SiC(0001), Phys. Rev. B - Condens. Matter Mater. Phys. 85 (2012) 1–7. doi:10.1103/PhysRevB.85.045418.

[21] M.G. Silly, G. Li, Y.J. Dappe, Electronic properties of zero-layer graphene on 6H-SiC(0001) substrate decoupled by silicon intercalation, Surf. Interface Anal. 46 (2014) 1273–1277. doi:10.1002/sia.5574.

[22] S. Watcharinyanon, L. I. Johansson, C. Xia, J. Ingo Flege, A. Meyer, J. Falta, C. Virojanadara, Ytterbium Intercalation of Epitaxial Graphene Grown on Si-Face SiC, Graphene. 2 (2013) 66–73. doi:10.4236/graphene.2013.22010.

[23] H. Kim, O. Dugerjav, A. Arvisbaatar, J.M. Seo, Bifunctional effects of the ordered Si atoms intercalated between quasi-free-standing epitaxial graphene and SiC(0001): graphene doping and substrate band bending, New J. Phys. 17 (2015) 83058. doi:10.1088/1367-2630/17/8/083058.

[24] H. Kim, O. Dugerjav, A. Lkhagvasuren, J.M. Seo, Origin of ambipolar graphene doping induced by the ordered Ge fi lm intercalated on SiC (0001), Carbon 108 (2016) 154–164. doi:10.1016/j.carbon.2016.07.010.

[25] R. Addou, A. Dahal, M. Batzill, Graphene on ordered Ni-alloy surfaces formed by metal (Sn, Al) intercalation between graphene/Ni(111), Surf. Sci. 606 (2012) 1108–1112. doi:10.1016/j.susc.2012.03.009.

[26] N. Srivastava, G. He, P.C. Mende, R.M. Feenstra, Y. Sun, Luxmi, Graphene formed on SiC under various environments: Comparison of Si-face and C-face, J. Phys. D. Appl. Phys. 45 (2011) 21. doi:10.1088/0022-3727/45/15/154001.

[27] R. Nyholm, J.N. Andersen, U. Johansson, B.N. Jensen, I. Lindau, Beamline I311 at MAX-LAB: A VUV/soft X-ray undulator beamline for high resolution electron spectroscopy, Nucl. Instruments Methods Phys. Res. Sect. A Accel. Spectrometers, Detect. Assoc. Equip. 467–468 (2001) 520–524. doi:10.1016/S0168-9002(01)00399-0.

[28] S. Tanuma, C.J. Powell, D.R. Penn, Calculations of electron inelastic mean free paths. IX. Data for 41 elemental solids over the 50 eV to 30 keV range, Surf. Interface Anal. 43 (2011) 689–713. doi:10.1002/sia.3522.

[29] K. Von Bergmann, M. Bode, R. Wiesendanger, Magnetism of iron on tungsten (001) studied by spin-resolved scanning tunneling microscopy and spectroscopy, Phys. Rev. B - Condens. Matter Mater. Phys. 70 (2004) 1–10. doi:10.1103/PhysRevB.70.174455.

[30] W. B. Pearson, The crystal chemistry and physics of metals and alloys, Wiley-Interscience, John Wiley & Sons, Inc., New York-London-Sydney-Toronto (1972) 806.

[31] R.M. Feenstra, N. Srivastava, Q. Gao, M. Widom, B. Diaconescu, T. Ohta, G.L. Kellogg, J.T. Robinson, I. V. Vlassiouk, Low-energy electron reflectivity from graphene, Phys. Rev. B - Condens. Matter Mater. Phys. 87 (2013) 1–4. doi:10.1103/PhysRevB.87.041406.

[32] H. Hibino, H. Kageshima, F. Maeda, M. Nagase, Y. Kobayashi, H. Yamaguchi, Microscopic thickness determination of thin graphite films formed on SiC from quantized oscillation in reflectivity of low-energy electrons, Phys. Rev. B - Condens.

Matter Mater. Phys. 77 (2008) 1–7. doi:10.1103/PhysRevB.77.075413.

[33] LEEM-IV curves of n-type and p-type Au intercalated buffer layer graphene, (unpublished data).

[34] H. Kim, O. Dugerjav, A. Lkhagvasuren, J.M. Seo, Charge neutrality of quasi-free-standing monolayer graphene induced by the intercalated Sn layer, J. Phys. D. Appl. Phys. 49 (2016) 135307. doi:10.1088/0022-3727/49/13/135307.

[35] V.M. Mikoushkin, V. V. Shnitov, A. A. Lebedev, S. P. Lebedev, S.Y. Nikonov, O.Y. Vilkov, T. Iakimov, R. Yakimova, Size confinement effect in graphene grown on 6H-SiC (0001) substrate, Carbon N. Y. 86 (2014) 7. doi:10.1016/j.carbon.2015.01.015.

[36] J.M. Themlin, M. Chtaib, L. Henrard, P. Lambin, J. Darville, J.M. Gilles, Characterization of tin oxides by x-ray-photoemission spectroscopy, Phys. Rev. B. 46 (1992) 2460–2466. doi:10.1103/PhysRevB.46.2460.

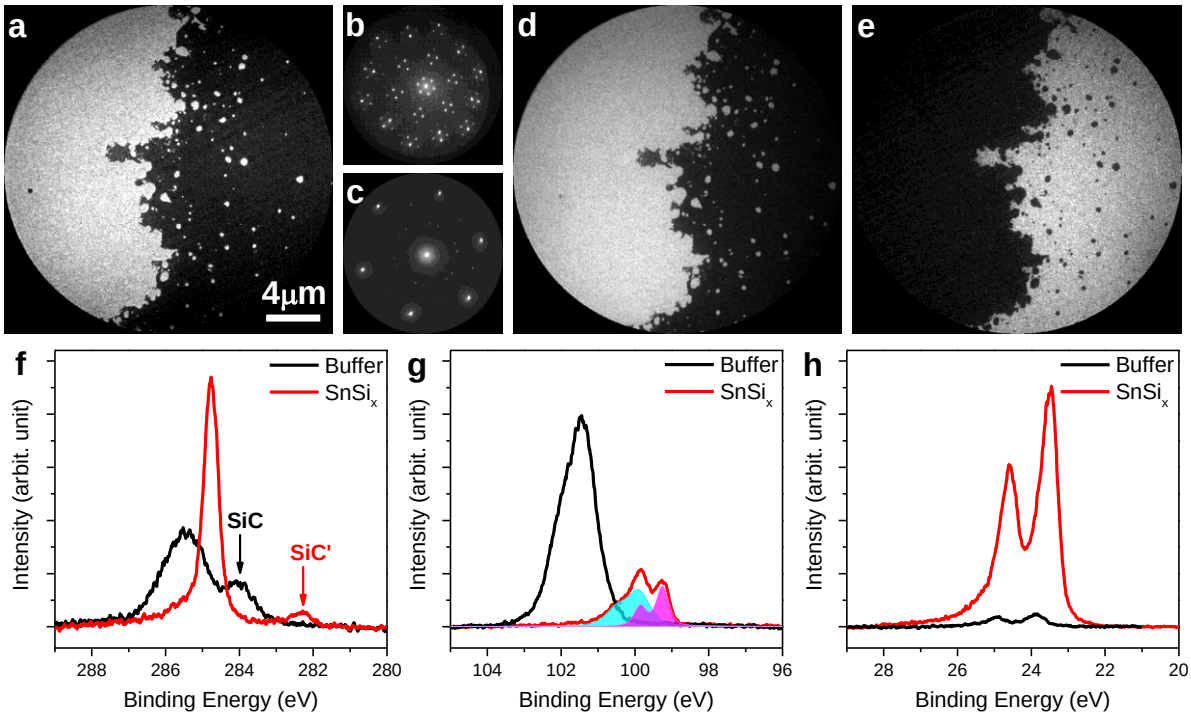

Fig.1. (a) LEEM, (d) Si2p XPEEM and (e) Sn4d XPEEM images measured at room temperature at the boundary between the buffer layer area (left) and the $SnSi_x$ intercalated area (right) after the sample was gradually heated up to 1050 °C. LEED patterns of the two areas are shown in (b) and (c). The imaging electron energy is 4.9 eV in (a) and 45 eV in μ-LEED. The imaging (photon) energy is 101.26 eV (133 eV) in (d) and 23.23 eV (80 eV) in (e). (f)–(h) μ-XPS spectra of (f) C1s, (g) Si2p and (h) Sn4d measured from both halves, about 40 μm away from the boundary. The photon energy is 330 eV in (f), 150 eV in (g) and 60 eV in (h). The arrows in (f) indicate that the bulk C1s components from SiC substrate have moved to the lower binding energy by 1.6 eV when the buffer layer (SiC) was transferred to a quasi-free-standing graphene (SiC') by Sn intercalation. In (g), Si2p spectrum after Sn intercalation is fitted by two contributions: one from the bulk SiC (cyan) and the other from Si-Sn bonds (magenta).

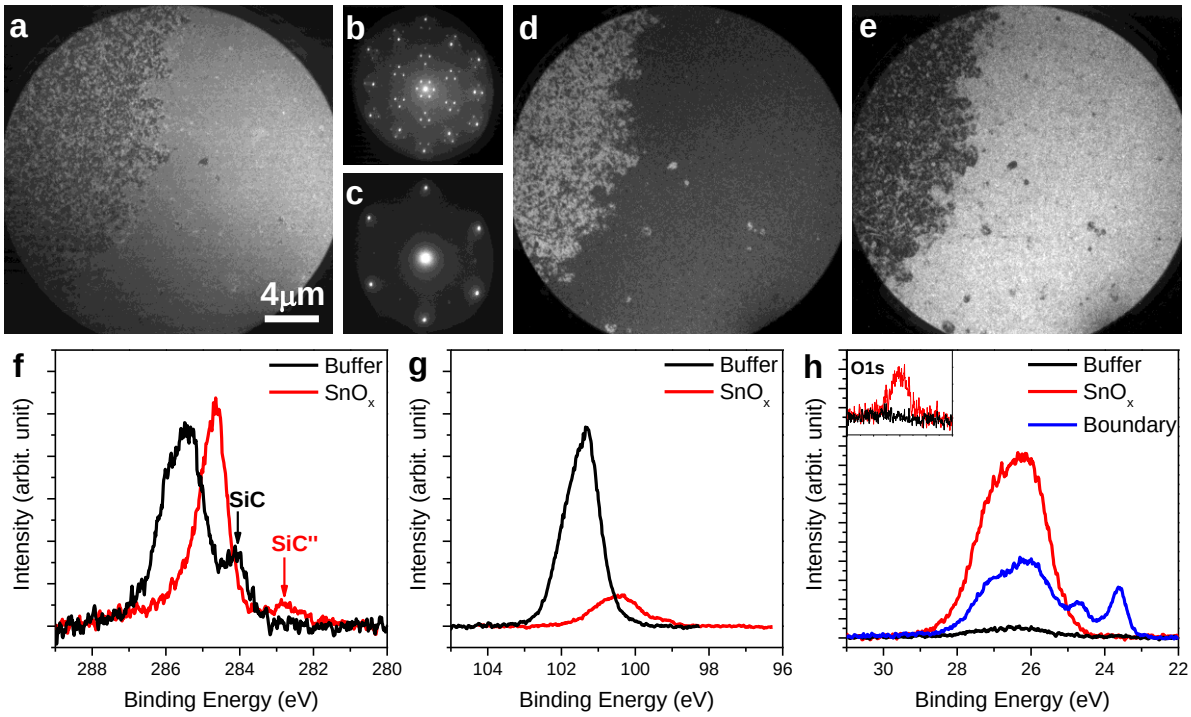

Fig.2. (a) LEEM, (d) Si2p XPEEM and (e) Sn4d XPEEM images acquired at the boundary between the buffer layer area (left) and the Sn-intercalated area (right) after long time exposure at ambient pressure. LEED patterns of the two areas are shown in (b) and (c). The imaging electron energy is 1.8 eV in (a) and 45 eV in μ-LEED. The binding (photon) energy is 101.28 eV (133 eV) in (d) and 25.75 eV (90 eV) in (e). (f)–(h) μ-XPS spectra of (f) C1s, (g) Si2p and (h) Sn4d measured from both halves, about 150 μm away from the boundary. The photon energy is 330 eV in (f), 133 eV in (g) and 60 eV in (h). The arrows indicate the bulk C1s components of the buffer layer area (SiC) and the SnO_x intercalated graphene (SiC"). The inset in (h) shows O1s spectra from two areas taken at photon energy of 600 eV.

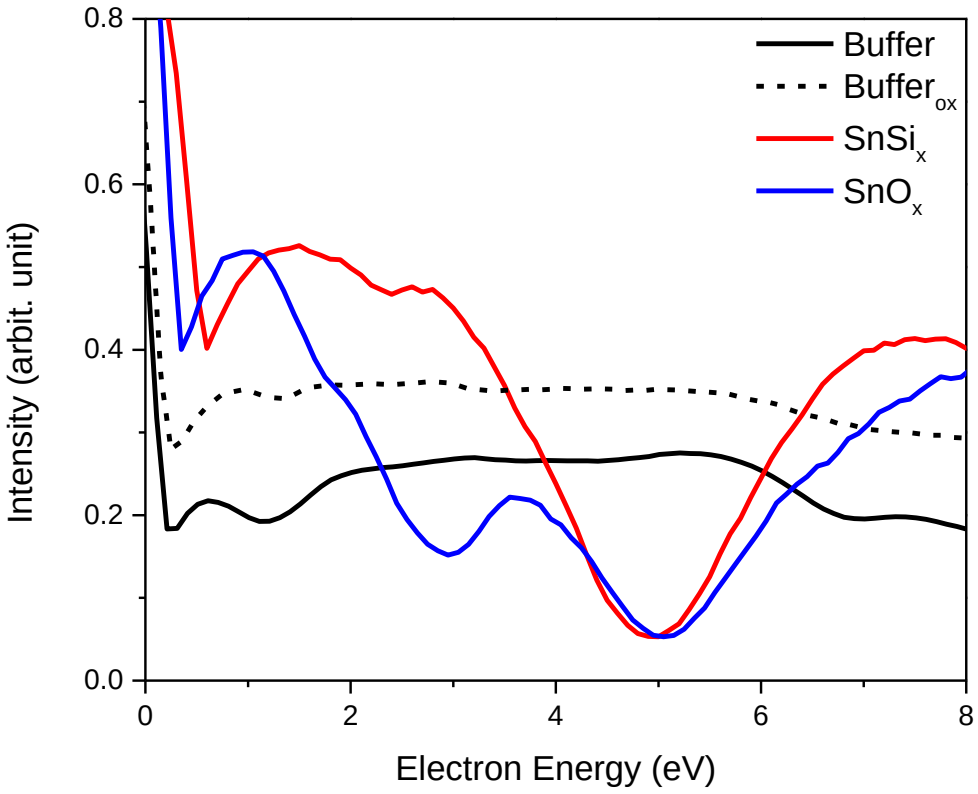

Fig.3. LEEM-IV curves from the pristine buffer layer, the buffer layer after oxidation, $SnSi_x$ and SnO_x intercalated graphene. Each curve has been normalized to the total reflection (R=1) at zero or negative electron energy. The curve of the buffer layer after oxidation, $Buffer_{ox}$, has been shifted vertically for a better viewing and comparison.

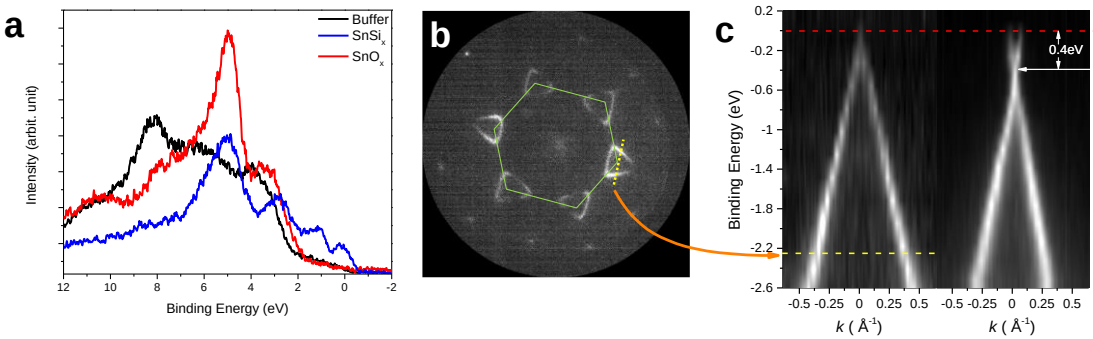

Fig.4. (a) Valence band spectra ($h\nu$= 60 eV) of the buffer layer, Sn intercalated graphene and Sn oxide intercalated graphene. (b) a μ-ARPES ($h\nu$= 45 eV) (k_x,k_y) map (E_B= –2.25 eV) which clearly shows the emergence of Dirac cones from the graphene after Sn intercalation. (c) $E(k)$ for $SnSi_x$ intercalated graphene (left) and SnO_x intercalated graphene (right) after re-slicing along the yellow line drawn in (b). The yellow line in (c) marks the energy where the μ-ARPES image in (b) was taken.

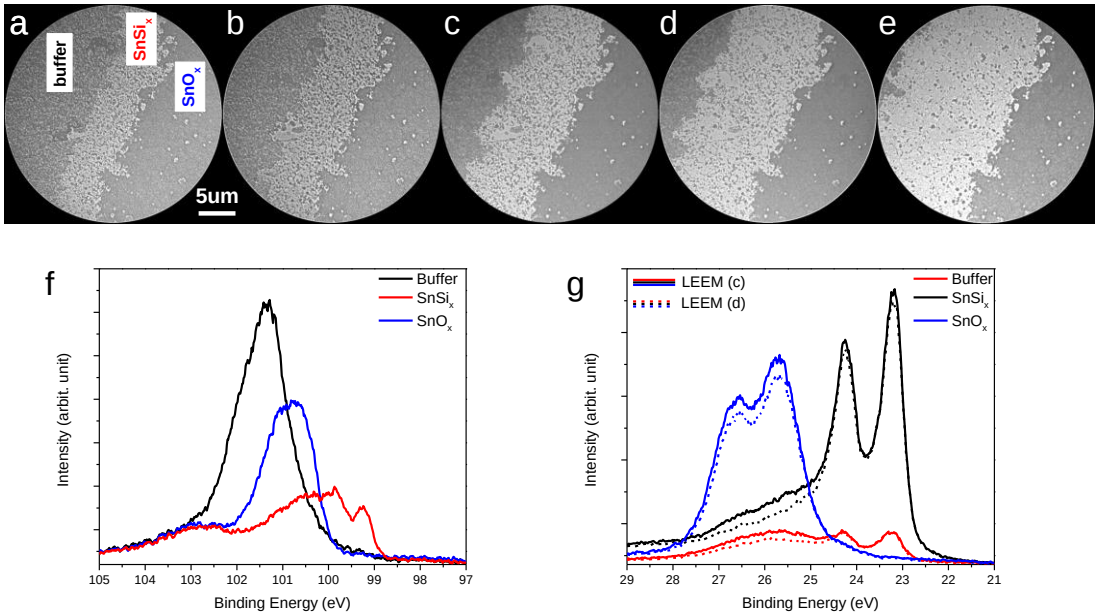

Fig.5. (a-e) LEEM images taken during successive flashes at 1100 °C showing the formation of the metallic $SnSi_x$ intercalated graphene area (middle) that results from decomposition of small patches of the SnO_x intercalated graphene. (f) Si2p and (g) Sn4d spectra taken from the three areas in the middle (c) LEEM image. The dash lines in (g) represent the set of data from the next (d) LEEM image showing the process of SnO_x decomposition.